CLUSTERING OF INTERMEDIATE-LUMINOSITY X-RAY–SELECTED ACTIVE GALACTIC NUCLEI AT $z \sim 3$[1]

Harold Francke,[2,3] Eric Gawiser,[3,4,5] Paulina Lira,[2] Ezequiel Treister,[6] Shanil Virani,[3] Carie Cardamone,[3] C. M. Urry,[5] Pieter van Dokkum,[3] and Ryan Quadri[3]

ABSTRACT

We present the first clustering results of X-ray–selected active galactic nuclei (AGNs) at $z \sim 3$. Using *Chandra* X-ray imaging and *UVR* optical colors from MUSYC photometry in the Extended Chandra Deep Field–South field, we selected a sample of 58 $z \sim 3$ AGN candidates. From the optical data we also selected 1385 luminous blue galaxies (LBGs) at $2.8 < z < 3.8$ with $R < 25.5$. We performed autocorrelation and cross-correlation analyses, and here we present results for the clustering amplitudes and dark matter (DM) halo masses of each sample. For the LBGs we find a correlation length of $r_{0,\mathrm{LBG}} = 6.7 \pm 0.5$ Mpc, implying a bias value of 3.5 ± 0.3 and DM halo masses of $\log(M_{\mathrm{min}}/M_{\odot}) = 11.8 \pm 0.1$. The AGN-LBG cross-correlation yields $r_{0,\mathrm{AGN\text{-}LBG}} = 8.7 \pm 1.9$ Mpc, implying for AGNs at $2.8 < z < 3.8$ a bias value of 5.5 ± 2.0 and DM halo masses of $\log(M_{\mathrm{min}}/M_{\odot}) = 12.6^{+0.5}_{-0.8}$. Evolution of DM halos in the ΛCDM cosmology implies that today these $z \sim 3$ AGNs are found in high-mass galaxies with a typical luminosity of $7^{+4}_{-2}L^*$.

Subject headings: galaxies: active — galaxies: high-redshift — large-scale structure of universe

On-line material: color figure

1. INTRODUCTION

There is a wealth of evidence that nuclear supermassive black holes play a significant role in the process of galaxy formation and evolution. This has become evident in the past few years with the discovery of correlations between the properties of the massive black holes, the stellar systems that host them, and their dark matter halos (Magorrian et al. 1998; Gebhardt et al. 2000; Ferrarese 2002).

Luminous quasars have been studied in great detail, with systematic spectroscopic studies by the Sloan Digital Sky Survey and the 2dF Galaxy Redshift Survey. These objects are rare and represent the bright end of the active galactic nuclei (AGN) luminosity function. In order to fully understand the link between the growth of supermassive black holes (SMBHs) and galaxy evolution, we need to study young, high-redshift galaxies hosting AGNs with more typical luminosities.

One of the basic properties of galaxy populations is their clustering strength, but there are few constraints on this quantity for fainter, high-redshift AGNs. Furthermore, there are important disagreements in the literature: e.g., galaxy-AGN cross-correlation measurements at $z \sim 3$ by Adelberger & Steidel (2005b) imply a bias factor of 3.9 ± 3.0 for luminous AGNs (*UV* luminosities in the range $-30 < M_{1350} < -25$), while recent work by Shen et al. (2007) suggests a value of 9.1 ± 0.9 for sources with similar luminosities at the same redshift. For galaxies, e.g., measurements indicate a strong luminosity dependence in the clustering length (Giavalisco & Dickinson 2001). On the other hand, for AGNs there are a handful of claims that this is not the case (Croom et al. 2005; Myers et al. 2006; Adelberger & Steidel 2005a). Determining the bias with accuracy puts important constraints on models of AGN formation and evolution (e.g., Lidz et al. 2006; Hopkins et al. 2007) but requires spanning a broad range in luminosity and obscuration level. This is challenging using optical color selection plus spectroscopy, because the low fraction of AGNs (3%) found among these candidates (Steidel et al. 2002) demands huge amounts of spectroscopy time. Using X-ray detection plus spectroscopy (e.g., Szokoly et al. 2004) provides a more efficient and unbiased selection of AGNs, since their surface density is higher in X-rays than in optical images and obscuration effects are much less important. However, the unrestricted redshift range sampled by this method makes spectroscopic follow-up highly inefficient and often prevents confirmation of dimmer, high-z AGNs ($R > 24$). Hence it is difficult to obtain AGN samples suitable for clustering studies. There have been several measurements of the spatial correlation function of X-ray–selected AGNs at $z < 1$ (Mullis et al. 2004; Gilli et al. 2005, Basilakos et al. 2004, 2005; Yang et al. 2006; Miyaji et al. 2007), with samples ranging from 200 to 500 sources. At higher redshifts, the statistics are much poorer and consist of purely optically selected AGNs. In this work, we constrain the clustering strength of an AGN sample at $z \sim 3$ jointly selected by optical and X-ray photometry. We determine whether these sources cluster more or less than nonactive galaxies at this redshift and discuss their present-day descendants.

We assume a ΛCDM cosmology consistent with *WMAP* results (Spergel et al. 2007) with $\Omega_m = 0.3$, $\Omega_\Lambda = 0.7$, $H_0 = 70$ km s^{-1} Mpc^{-1}, and $\sigma_8 = 0.8$. All quantities are comoving: correlation lengths scale as h_{70}^{-1}, number densities as h_{70}^{3}, and halo masses as h_{70}^{-1}.

2. OBSERVATIONS

The MUSYC survey was optimized to study galaxies at $z \sim 3$, with imaging depths down to the spectroscopic limit, U,

[1] This work is based on observations made with the 6.5 m Magellan-Baade telescope, a collaboration between the Observatories of the Carnegie Institution of Washington, University of Arizona, Harvard University, University of Michigan, and Massachusetts Institute of Technology, and at Cerro Tololo Inter-American Observatory, a division of the National Optical Astronomy Observatory, which is operated by the Association of Universities for Research in Astronomy, Inc., under cooperative agreement with the National Science Foundation.

[2] Departamento de Astronomía, Universidad de Chile, Casilla 36-D, Santiago, Chile; hfrancke@das.uchile.cl.

[3] Department of Astronomy, Yale University, P.O. Box 208101, New Haven, CT 06520.

[4] Department of Physics and Astronomy, Rutgers University, 136 Frelinghuysen Road, Piscataway, NJ 08854-8019.

[5] Yale Center for Astronomy and Astrophysics and Department of Physics, Yale University, P.O. Box 208121, New Haven, CT 06520.

[6] European Southern Observatory, Santiago, Chile.

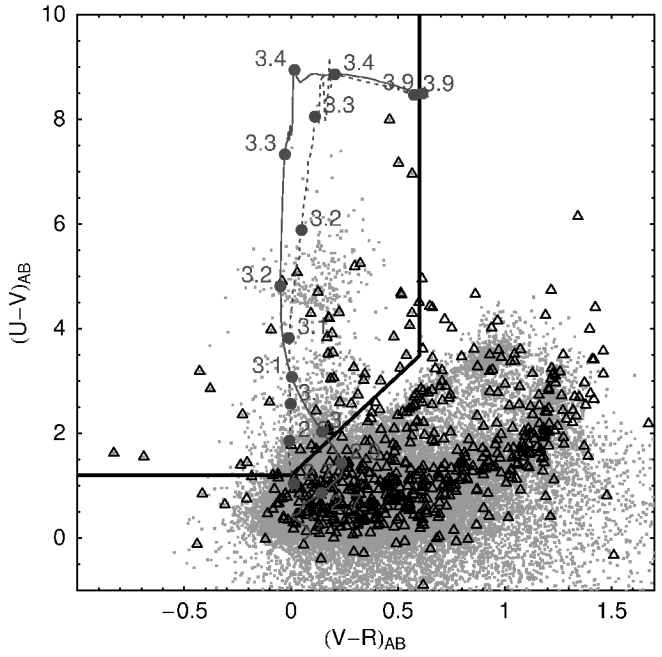

FIG. 1.—$U-V$ vs. $V-R$ color-color plot for all the sources brighter than $R = 25.5$ in the MUSYC ECDF-S optical catalog (*gray points*) and X-ray counterparts (*open triangles*). LBGs and $z \sim 3$ AGNs are inside the region marked in solid lines. The color-color tracks of a template AGN and an LBG as they are redshifted from $z = 2.0$ to 3.9 are shown in the red solid and blue dotted curves, respectively. [*See the electronic edition of the Journal for a color version of this figure.*]

B, V, $R \sim 26$ (Gawiser et al. 2006b). In the Extended Chandra Deep Field–South (ECDF-S) field, in particular, the 5 σ limiting (AB) magnitudes achieved in these bandpasses are 26.0, 26.9, 26.4, and 26.4, respectively. The main MUSYC catalog is based on the sources detected on the combined *BVR* image, and aperture photometry is performed on each filter in those positions (see Gawiser et al. 2006a).

The deep *Chandra* observations of this field have produced four X-ray catalogs: Giacconi et al. (2002), Alexander et al. (2003), Lehmer et al. (2005), and Virani et al. (2006). The first two comprise 1 Ms of exposures inside the central region (CDF-S proper), covering an area of $\approx$0.1 deg^2 (PI R. Giacconi). The Alexander et al. catalog has reported flux limits of 5.2×10^{-17} ergs cm^{-2} s^{-1} and 2.8×10^{-16} ergs cm^{-2} s^{-1} in the soft (0.5–2 keV) and hard (2–8 keV) bands, respectively. The last two catalogs come from the four $\approx$250 ks pointings that cover an area of $\approx$0.3 deg^2 around the former field (PI N. Brandt). Limiting X-ray fluxes in the extended region are 1.1×10^{-16} ergs cm^{-2} s^{-1} in the soft band and 6.7×10^{-16} ergs cm^{-2} s^{-1} in the hard band.

The MUSYC spectroscopic follow-up program carried out with Magellan/Baade+IMACS has yielded 280 successful identifications of $z > 2$ galaxies. Data were obtained with a resolution of $R = 640$ (470 km s^{-1} at 5000 Å) and slitlets of 1.2″ (P. Lira et al., in preparation). The broad wavelength coverage provided by IMACS, between 4000 and 9000 Å, allows the detection of Lyα and C IV 1549, the two most prominent ultraviolet AGN emission lines, at redshifts $2.3 < z < 4.0$.

3. AGN AND LBG SAMPLES

The full set of unique X-ray counterparts is taken from the MUSYC ECDF-S X-ray catalog (Cardamone et al. 2007), constructed by joining the catalogs from Giacconi et al. (2002), Alexander et al. (2003), Virani et al. (2006), and Lehmer et al. (2005) using a likelihood procedure (Brusa et al. 2005) to match sources between the X-ray and optical (*BVR*-selected) catalogs.

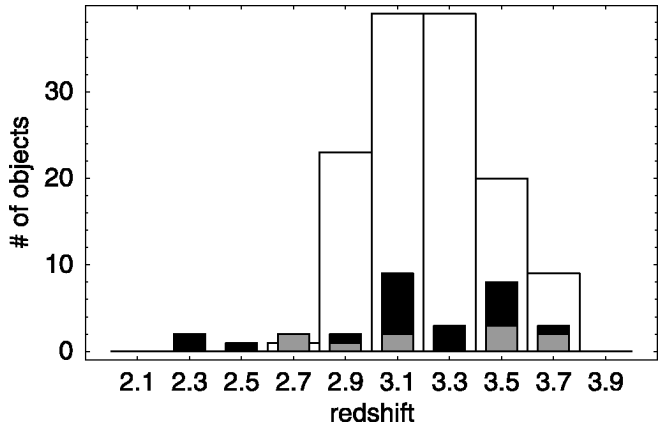

FIG. 2.—Redshift distribution of all spectroscopically confirmed LBGs (*white bars*) and $z \sim 3$ AGNs (*black bars*) in MUSYC. The subset of AGNs in ECDF-S is in gray bars. These distributions have mean and variances $z_{\rm AGN} = 3.18$, $\sigma_{z,\rm AGN} = 0.39$, $z_{\rm LBG} = 3.23$, and $\sigma_{z,\rm LBG} = 0.22$.

Figure 1 shows the $U-V$ versus $V-R$ color-color plot for sources in the ECDF-S from MUSYC photometry. Lyman-break color selection (*UVR*) corresponds to the region outlined in the upper left side (Steidel et al. 1996; Gawiser et al. 2006a). For this color selection, *U*-band fluxes are required to be detected at 1 σ and are otherwise set to an upper limit equal to their 1 σ error. This avoids interlopers (typically dwarf stars) with uncertain photometry at the cost of incompleteness in the sample. Additionally, $R < 25.5$ is required to allow for spectroscopic confirmation. Sources presenting a drop in the *U* filter due to intergalactic absorption, along with a blue continuum between the *V* and *R* filters that rules out heavily reddened lower-z objects, are expected to lie at $2.7 < z < 3.7$. For X*UVR* selection of AGNs, we require an X-ray detection with counterpart *UVR* colors in the same region, and we drop the *R* magnitude limit and the 1 σ *U*-band requirement, since the extra requirement of X-ray emission already rules out most dwarf stars. This procedure yields 1385 LBG and 58 AGN candidates. Unobscured AGNs and LBGs have somewhat similar *UVR* colors, as can be seen in the color-color track in Figure 1, since these colors are mainly determined by the intergalactic hydrogen absorption. Furthermore, obscured AGNs are the dominant population among AGNs, and since the spectral energy distribution of the first is dominated by their host galaxies (Treister et al. 2004; Treister & Urry 2005), we expect the redshift distribution of our AGN sample to differ mildly from the LBG distribution. Notice that in the case of significant obscuration, we do not expect to select AGNs hosted by very red galaxies, since they will probably not be bright enough in the rest-frame *UV*.

From the spectra obtained over the entire four-field survey so far, 131 LBGs and 30 AGNs were identified at the target redshift $\sim$3, and in the ECDF-S in particular, 31 LBGs and 11 AGNs have been confirmed. While AGNs in the ECDF-S were directly targeted using a joint X-ray and optical selection, in the rest of the MUSYC fields AGNs have been discovered serendipitously among the *UVR* candidates (see Fig. 1). Figure 2 shows the redshift histograms of the confirmed objects, which implies X-ray luminosities between 10^{43} and 10^{45} ergs s^{-1} for the entire set of AGN candidates. The Lyman-break (*UVR*) selection shows a fraction of low-redshift interloper less than

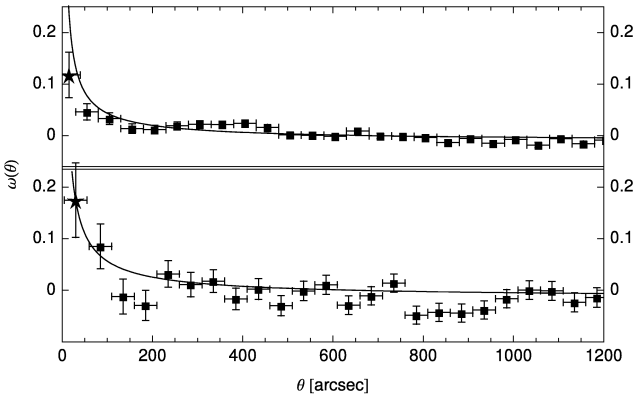

FIG. 3.—*Top:* Angular autocorrelation function for *UVR* selected sources, i.e., Lyman-break galaxies at $z \sim 3$. The solid line is the best fit to the data, $\omega_{\rm LBG}(\theta) = 2.2 \pm 0.3\ \theta^{-0.8}$. The point marked with a star is not included in the fit and is shown only for reference. *Bottom:* Analogous plot for the angular cross-correlation function with X*UVR* sources, i.e., AGNs at $z \sim 3$. The best fit corresponds to $\omega_{\rm AGN\text{-}LBG}(\theta) = 2.9 \pm 1.1\ \theta^{-0.8}$.

10%. In the spectra of the X*UVR*-targeted AGNs in ECDF-S, we did not observe any interlopers.

4. CLUSTERING ANALYSIS

We calculate the clustering of AGNs via a two-step method, calculating the autocorrelation of LBGs first and then their cross-correlation with AGNs. The main advantage of this approach is that it improves the statistics significantly, since the LBG population is much more numerous and its redshift distribution is similar to the AGN population sampled here, and the AGN-LBG cross-correlation function is less noisy than the AGN autocorrelation function (Kauffmann & Haehnelt 2002). Notice that the AGNs and LBGs that contribute to the cross-correlation function will be those that spatially overlap. Therefore, our results will reflect the clustering of AGNs in the redshift range $2.7 < z < 3.8$.

For the *UVR*-selected sources, we calculated the angular autocorrelation function using the Landy & Szalay (1993) estimator:

$$\hat{\omega}_{\rm LS}(\theta) = \frac{\rm DD(\theta) - 2DR(\theta) + RR(\theta)}{\rm RR(\theta)}, \qquad (1)$$

where DD, DR, and RR are the data-data, data-random, and random-random pairs, all normalized to integrate to 1. To estimate the angular cross-correlation between *UVR*-X*UVR* sources, we used the following cross-correlation estimator (Croft et al. 1999):

$$\hat{\omega}_{\rm AGN\text{-}LBG}(\theta) = \frac{D_{\rm AGN}D_{\rm LBG}(\theta)}{D_{\rm AGN}R_{\rm LBG}(\theta)} - 1, \qquad (2)$$

where now the data-data pairs are between AGNs and LBGs and data-random between AGNs and the optical random catalog. Notice that this estimator does not use a random catalog for the X-ray sources. The degradation of the point-spread function and sensitivity as a function of the off-axis angle in the *Chandra* data makes the X-ray survey geometry fairly complicated, but these resulting systematic uncertainties can be avoided in this cross-correlation scheme.

The estimates shown above were fitted to $\hat{\omega}(\theta) = A\theta^{-\beta} - {\rm IC}(A, \beta)$, where the integral constraint factor IC is included as part of the model and we assumed the usual power law for the true angular correlation function. We kept $\beta = 0.8$ fixed since our signal-to-noise ratio (S/N) does not allow us to put significant constraints on the slope. Fit limits have been set to avoid the one-halo term regime on small angular scales (30″ for LBGs and 60″ for AGNs based on the virial radii of their initially inferred DM halo masses of 6×10^{11} and $10^{13} M_\odot$, respectively) and ending at half the field size on the larger scales, in order to avoid border effects of the estimator and where the sampling becomes poor anyway. The fit to the LBG autocorrelation function gave $A_{\rm LBG} = 2.2 \pm 0.3$ arcsec$^\beta$ and the fit to the cross-correlation function $A_{\rm AGN\text{-}LBG} = 2.9 \pm 1.1$ arcsec$^\beta$, with reduced χ^2 values of 1.24 and 1.21, respectively. The errors in these parameters were calculated using $\Delta\chi^2$ and correspond to 1 σ confidence level with one parameter. Figure 3 shows the measured angular correlation functions with their corresponding best-fit models. Binning $\omega(\theta)/\sigma_\omega(\theta)$ over the entire fitting range gives estimates for the total S/Ns of these measurements of 10.2 and 3.9, correspondingly. From Monte Carlo realizations, we estimated that the probabilities of obtaining clustering this high from unclustered populations of the same sizes are <0.1% for the LBG autocorrelation and 1% for the AGN-LBG cross-correlation.

Using smooth fits to the redshift distributions of the confirmed sources shown in Figure 2, we deprojected the values obtained for the angular LBG autocorrelation and LBG-AGN cross-correlation amplitude using Limber's equation. We obtained spatial correlation lengths of $r_{0,\rm LBG} = 6.7 \pm 0.5$ Mpc and $r_{0,\rm AGN\text{-}LBG} = 8.7 \pm 1.9$ Mpc, respectively, where the correlation length is defined by the usual fitting form $\xi(r) = (r/r_0)^{-\gamma}$ for the spatial correlation function. The random errors introduced in the deprojection are included in the error budget by approximating the redshift distributions as Gaussians and propagating the standard errors in their means and variances.

To calculate the bias factor of the AGN sample in the approximation of linear, constant bias, we used the elementary relations $b^2_{\rm LBG} = \sigma^2_{8,\rm LBG}/\sigma^2_{8,\rm DM}$ and $b_{\rm AGN} b_{\rm LBG} = \sigma^2_{8,\rm AGN\text{-}LBG}/\sigma^2_{8,\rm DM}$, where $\sigma^2_{8,X}$ is the variance in spheres of radius 8 h^{-1}_{100} Mpc in the random field described by the corresponding auto- or cross-correlation function. Although A/β and r_0/γ are highly degenerate parameter pairs, the bias factors are robust to variations in the slope β (or γ). Therefore, they are our preferred quantity for comparison with the literature. The bias, number densities, and masses shown in Table 1 are calculated using the ellipsoidal collapse model extension of the Press-Schechter formalism by Sheth & Tormen (1999) and the extension of the Mo & White (1996) formalism by Sheth et al. (2001). These quantities were evaluated at the mean redshifts of the confirmed samples, both very close to $z = 3.2$.

TABLE 1

SUMMARY OF DARK MATTER HALO PROPERTIES

Sample	Bias	$\log(M_{\rm min})$	$n_{\rm halo}$ (Mpc^{-3})
LBG	3.5 ± 0.3	11.8 ± 0.15	$9 \pm 4 \times 10^{-4}$
AGN	5.5 ± 2	$12.6^{+0.5}_{-0.8}$	10^{-3}–10^{-6}

NOTE.—Confidence intervals/ranges are 1 σ. Masses are given in logarithm of solar masses.

5. DISCUSSION

We have measured the autocorrelation strength of $z = 3$ LBGs and the cross-correlation between these galaxies and

AGNs selected using both X-ray and optical data. For the LBG sample, we obtained a bias factor of 3.5 ± 0.3. This is somewhat higher than the value of 2.8 ± 0.3 found by Adelberger et al. (2005) at $z = 3$. Hildebrandt et al. (2007) obtained a bias value of 3.2 ± 0.2 for an equivalent LBG population, consistent with ours.

From the AGN-LBG cross-correlation and the bias calculated for the LBGs, we have deduced a bias factor of 5.5 ± 2 for our AGN sample. The active galaxies targeted in this study appear to cluster more than star-forming galaxies with similar rest-frame *UV* colors. This is consistent with cosmic downsizing of AGNs, implying that typical SMBHs tend to sit in more massive galaxies than the "normal" galaxy population. We need greater statistics to confirm this result, since the values are consistent within the uncertainties.

Adelberger & Steidel (2005b) performed this same calculation in an optically selected and spectroscopically confirmed sample of 79 AGNs between $1.6 < z < 3.7$, dividing the AGNs by *UV* luminosity into bright (25 sources with $-30 < M_{1350} < -25$) and dim (54 sources with $-25 < M_{1350} < -19$) samples. Although Adelberger & Steidel (2005b) do not report the autocorrelation length of the galaxy sample used to compute these values, we approximate it by averaging the result for LBG and BX galaxies presented in Adelberger et al. (2005) obtaining a bias factor of 2.6 ± 0.3. From this we infer bias factors of 3.9 ± 3.0 and 4.7 ± 1.7 for the Adelberger & Steidel (2005b) bright and dim AGN samples. Our AGN sample has a *UV* magnitude range between −26 and −20, almost identical to the Adelberger & Steidel (2005b) faint AGN set and showing the same clustering strength. In Figure 4 these results are compared to the present estimate and to that obtained by Shen et al. (2007) for ∼2250 SDSS quasars at $2.9 < z < 3.5$.

To estimate the dark matter halo mass of the typical descendant of the halos that host these $z \sim 3$ galaxy sets at the present time, we calculated the mode and width of the conditional probability distribution of the expected mass $z = 0$ (see Hamana et al. 2006 and references therein). We took the median mass of the halo populations at $z = 3.2$ as the representative value, and we report the bias values corresponding to the maximum likelihood $z = 0$ progenitor, with 1 σ uncertainties corresponding to halo masses whose likelihood is reduced by a factor $\exp(-1/2) = 0.607$. For the LBG bias of 3.5 at $z = 3.2$, we obtain a bias of $1.3^{+0.3}_{-0.1}$ at $z = 0$. In the nearby universe (Zehavi et al. 2005), this corresponds to the clustering of a somewhat massive galaxy, with $L = 2.7^{+1.9}_{-0.6} L^*$. On the other hand, our AGN sample, with a bias of 5.5 at $z = 3.2$, would have a typical halo with a bias factor of $2.0^{+0.6}_{-0.3}$ at present. Extrapolating from Zehavi et al. (2005), this corresponds to the clustering of galaxies having $7^{+4}_{-2} L^*$, which at the present time are most likely located in groups and galaxy clusters.

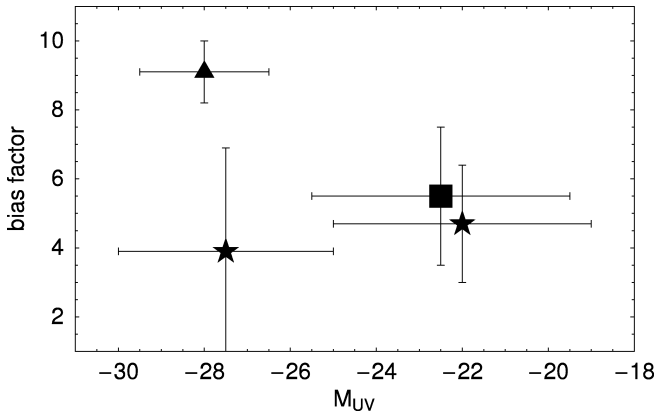

FIG. 4.—Comparison of AGN bias factors at $z \sim 3$ between this work (*square*), Shen et al. (2007) (*triangle*), and Adelberger & Steidel (2005b) (*stars*).

This confirms the result found by Adelberger & Steidel (2005b) for faint, optically selected AGNs. Improving our understanding of the AGN-galaxy connection at $z \sim 3$ and constraining models such as Lidz et al. (2006) and Hopkins et al. (2007) for AGN clustering requires resolving the discrepancy in the bias estimates for bright AGNs seen in Figure 4 by improving the statistics. We have show that targeting high-redshift AGNs for clustering analyses can be done very efficiently by means of deep optical and X-ray imaging, and for that reason, future surveys with deep X-ray coverage will be ideal for obtaining large samples of active galaxies in restricted redshift ranges, suitable for clustering studies. Our method can be applied to these surveys to obtain enough X-ray–selected AGNs to reduce the current uncertainties.

H. F. was supported by MECESUP project UCH0118, Andes Fundation fellowship C-13798, ALMA fellowship 31060003, and Fondecyt project 1040719.

REFERENCES

Adelberger, K. L., & Steidel, C. C. 2005a, ApJ, 630, 50
———. 2005b, ApJ, 627, L1
Adelberger, K. L., et al. 2005, ApJ, 619, 697
Alexander, D. M., et al. 2003, AJ, 126, 539
Basilakos, S., et al. 2004, ApJ, 607, L79
———. 2005, MNRAS, 356, 183
Brusa, M., et al. 2005, A&A, 432, 69
Cardamone, C. N., et al. 2007, ApJ, submitted
Croft, R. A. C., Dalton, G. B., & Efstathiou, G. 1999, MNRAS, 305, 547
Croom, S. M., et al. 2005, MNRAS, 356, 415
Ferrarese, L. 2002, ApJ, 578, 90
Gawiser, E., et al. 2006a, ApJS, 162, 1
———. 2006b, ApJ, 642, L13
Gebhardt, K., et al. 2000, ApJ, 539, L13
Giacconi, R., et al. 2002, ApJS, 139, 369
Giavalisco, M., & Dickinson, M. 2001, ApJ, 550, 177
Gilli, R., et al. 2005, A&A, 430, 811
Hamana, T., et al. 2006, MNRAS, 369, 1929
Hildebrandt, H., et al. 2007, A&A, 462, 865
Hopkins, P. F., et al. 2007, ApJ, 662, 110
Kauffmann, G., & Haehnelt, M. 2002, MNRAS, 332, 529
Landy, S. D., & Szalay, A. S. 1993, ApJ, 412, 64
Lehmer, B. D., et al. 2005, ApJS, 161, 21
Lidz, A., et al. 2006, ApJ, 641, 41
Magorrian, J., et al. 1998, AJ, 115, 2285
Miyaji, T., et al. 2007, ApJS, 172, 396
Mo, H. J., & White, S. D. M. 1996, MNRAS, 282, 347
Mullis, C. R., et al. 2004, ApJ, 617, 192
Myers, A. D., et al. 2006, ApJ, 638, 622
Shen, Y., et al. 2007, AJ, 133, 2222
Sheth, R. K., Mo, H. J., & Tormen, G. 2001, MNRAS, 323, 1
Sheth, R. K., & Tormen, G. 1999, MNRAS, 308, 119
Spergel, D. N., et al. 2007, ApJS, 170, 377
Steidel, C. C., et al. 1996, ApJ, 462, L17
———. 2002, ApJ, 576, 653
Szokoly, G. P., et al. 2004, ApJS, 155, 271
Treister, E., & Urry, C. M. 2005, ApJ, 630, 115
Treister, E., et al. 2004, ApJ, 616, 123
Virani, S. N., et al. 2006, AJ, 131, 2373
Yang, Y., et al. 2006, ApJ, 645, 68
Zehavi, I., et al. 2005, ApJ, 630, 1